2014

Suspended particulate layers and internal waves over the southern Monterey Bay continental shelf: An important control on shelf mud belts?

JOURNAL OF GEOPHYSICAL RESEARCH: OCEANS, VOL. 119, 428–444, doi:10.1002/2013JC009360, 2014

Suspended particulate layers and internal waves over the southern Monterey Bay continental shelf: An important control on shelf mud belts?

Olivia M. Cheriton,[1] Erika E. McPhee-Shaw,[2] William J. Shaw,[3] Timothy P. Stanton,[3] James G. Bellingham,[4] and Curt D. Storlazzi[1]

Received 18 August 2013; revised 9 December 2013; accepted 22 December 2013; published 21 January 2014.

[1] Physical and optical measurements taken over the mud belt on the southern continental shelf of Monterey Bay, California documented the frequent occurrence of suspended particulate matter features, the majority of which were detached from the seafloor, centered 9–33 m above the bed. In fall 2011, an automated profiling mooring and fixed instrumentation, including a thermistor chain and upward-looking acoustic Doppler current profiler, were deployed at 70 m depth for 5 weeks, and from 12 to 16 October a long-range autonomous underwater vehicle performed across-shelf transects. Individual SPM events were uncorrelated with local bed shear stress caused by surface waves and bottom currents. Nearly half of all observed SPM layers occurred during 1 week of the study, 9–16 October 2011, and were advected past the fixed profiling mooring by the onshore phase of semidiurnal internal tide bottom currents. At the start of the 9–16 October period, we observed intense near-bed vertical velocities capable of lifting particulates into the middle of the water column. This "updraft" event appears to have been associated with nonlinear adjustment of high-amplitude internal tides over the mid and outer shelf. These findings suggest that nonlinear internal tidal motions can erode material over the outer shelf and that, once suspended, this SPM can then be transported shoreward to the middle and shallow sections of the mud belt. This represents a fundamental broadening of our understanding of how shelf mud belts may be built up and sustained.

Citation: Cheriton, O. M., E. E. McPhee-Shaw, W. J. Shaw, T. P. Stanton, J. G. Bellingham, and C. D. Storlazzi (2014), Suspended particulate layers and internal waves over the southern Monterey Bay continental shelf: An important control on shelf mud belts?, *J. Geophys. Res. Oceans*, *119*, 428–444, doi:10.1002/2013JC009360.

1. Introduction

[2] Continental shelves are known to be important regions for the recycling of carbon and nutrients. On continental shelves, particularly those of eastern boundary upwelling coasts, benthic exchange and the delivery of seafloor material into the water column play a crucial role in ecosystem functioning [e.g., *Bruland et al*., 2001; *Puig et al*., 2001]. Intermediate nepheloid layers (INLs) containing elevated concentrations of suspended particulate matter (SPM) have been observed at continental margins worldwide and are important for the transfer of energy and material such as sediment [*McCave et al*., 2001], nutrients [*Nédélec et al*., 2007], and organic material [*Inthorn et al*., 2006] from the shelf to the open ocean and deep-sea environment. INLs have been observed in and around submarine canyons [*Gardner*, 1989; *Durrieu de Madron*, 1994; *Ryan et al*., 2010; *Johnston et al*., 2011], over continental slopes, shelves, and near shelf breaks [*Pak et al*., 1980; *Dickson and McCave*, 1986; *Walsh and Nittrouer*, 1999; *McCave et al*., 2001; *McPhee-Shaw et al*., 2004; *Puig et al*., 2004; *Ribo et al*., 2013]. The SPM within INLs can be dispersed across large horizontal scales, delivering sediment far from its original source, and the lateral sediment flux within these detached SPM features has been estimated to exceed vertical settling fluxes of surface particulates, making them an important means of transporting sediment from shelves to continental slopes and deeper [*Walsh and Nittrouer*, 1999; *van Weering et al*., 2001; *McPhee-Shaw et al*., 2004]. However, these studies tracked INLs in only the *offshore* direction from their detachment sites. It remains unclear whether shelf-depth INLs also play a role in the overall transport and distribution of material upslope or onshore from the detachment site. Previous studies also

[1]U.S. Geological Survey, Pacific Coastal and Marine Science Center, Santa Cruz, California, USA.
[2]Moss Landing Marine Laboratories, California State University, Moss Landing, California, USA.
[3]Oceanography Department, Naval Postgraduate School, Monterey, California, USA.
[4]Monterey Bay Aquarium Research Institute, Moss Landing, California, USA.

Corresponding author: O. M. Cheriton, U.S. Geological Survey, Pacific Coastal and Marine Science Center, 400 Natural Bridges Dr., Santa Cruz, CA 95060, USA. (ocheriton@usgs.gov)

2169-9275/14/10.1002/2013JC009360

did not address temporal or event-scale variability of benthic-exchange features.

[3] INLs form when the SPM within a bottom nepheloid layer (BNL) becomes detached from immediate contact with the seafloor or bottom boundary layer and disperses laterally along isopycnals. There is increasing evidence that internal wave interaction with seafloor topography is an important mechanism for the formation of INLs; this has been documented by both field [*Cacchione and Drake*, 1986; *Bogucki et al*., 1997; *Johnson et al*., 2001; *McPhee-Shaw et al*., 2004; *Puig et al*., 2004; *Moum et al*., 2007] and laboratory studies [*Ivey and Nokes*, 1989; *Taylor*, 1993; *McPhee-Shaw and Kunze*, 2002]. *Cacchione and Drake* [1986] were one of the first to describe how the reflection of internal waves with critical slope regions of continental margins could result in intensified bottom velocities that could resuspend surficial seafloor particulates. In addition, both laboratory and field studies have found evidence that the internal tide may not only cause the initial detachment of SPM from the seafloor, but also its subsequent lateral dispersal and along-isopycnal transport [*McPhee-Shaw and Kunze*, 2002; *Johnston et al*., 2011].

[4] Surface wave-induced bed shear stresses are thought to control the majority of seabed material resuspension on the shallow shelf [*Sternberg and Larsen*, 1975]; indeed this mechanism has been identified as the primary control on the inshore boundary of fine-grained silts and clays comprising midshelf mud belts [*George and Hill*, 2008]. Enhanced currents near the shelf break and at critical regions of the shelf may also drive resuspension and transport of these fine particulates [*Cacchione and Southard*, 1974; *Noble and Xu*, 2003]. In addition to current-induced bed shear stress, the vertical velocities associated with the passage of energetic internal waves may also resuspend materials near the seabed [*Bogucki et al*., 1997]. Acoustic scattering particles on the outer Monterey Bay shelf were suggested to be associated with the passage of nonlinear internal waves [*Carter et al*., 2005]. It remains unknown whether boundary layer detachment and eventual SPM dispersal is primarily controlled by erosion and resuspension or whether, instead, convergent and advective dynamics in the water column well above the seafloor are more important in generating these features (see review by *McPhee-Shaw* [2006]).

[5] Here we present long-term, high-resolution observations of SPM over the southern Monterey Bay shelf. Observational objectives were to measure current velocities and the physical structure of the water column, including high-frequency internal waves, while simultaneously detecting and resolving near-bottom SPM features. Our goals were to (1) observe SPM patterns over the mid to outer shelf, (2) determine how SPM features vary in space and time, and (3) evaluate whether these layers are associated with particular processes such as erosion due to large surface waves or mixing or advection by internal waves.

2. Study Site

[6] Located on the central California coast, Monterey Bay is a large, open embayment bisected by the Monterey Submarine Canyon, which runs east to west through the middle of the Bay (Figure 1). Local hydrography is

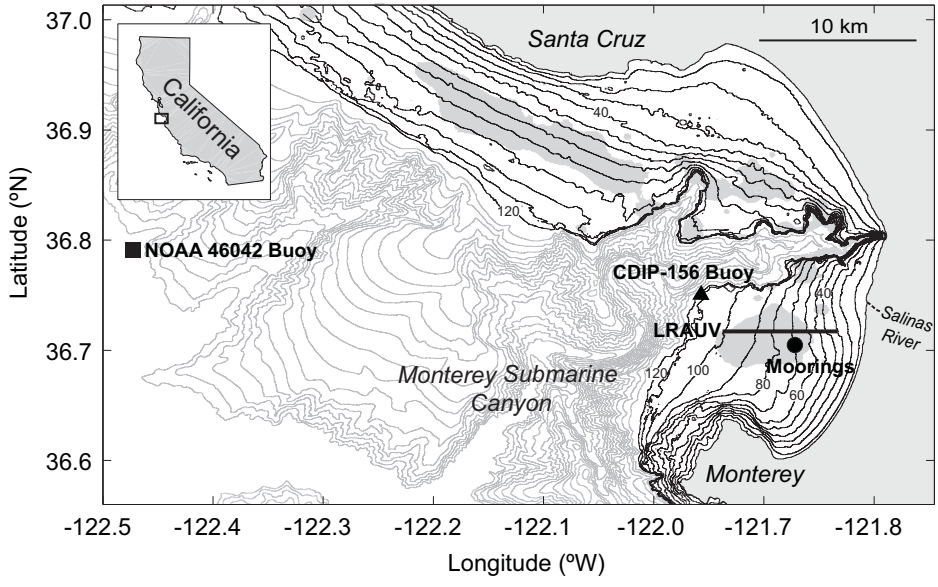

Figure 1. Map of study site in southern Monterey Bay. The thick black line is the path of the long-range autonomous underwater vehicle (LRAUV) transects, and the black circle is the site where the mooring instrument platforms (autonomous profiler, acoustic Doppler current profiler, and thermistor chain) were deployed. Locations of the NOAA 46042 (square) and CDIP-156 (triangle) buoys are also shown. Bathymetric contours are in 10 m steps from 0 to 120 m (black contours), and 100 m steps from 200 to 2000 m (gray contours). Also shown is the distribution seafloor sediment of diameter <34 μm (data originally published in *Edwards* [2002]), indicating the location of the midshelf mud belt in relation to our sampling platforms. The inset map shows the location of Monterey Bay along the coast of California, USA.

strongly controlled by offshore winds [*Breaker and Broenkow*, 1994]. The predominant northwesterly winds are strongest after the spring transition and drive the upwelling of cold, nutrient-rich waters from depth as deep as 300 m [*Rosenfeld et al*., 1994]. The relaxation or reversal of this wind pattern allows warm surface waters to move back in over the shelf. This study took place between late September and the end of October, a season considered a transition between the warm, well stratified late summer and fall and the more energetic winter period of storms and intense but variable winds [*Skogsberg*, 1936; *Largier et al*., 1993; *Pennington and Chavez*, 2000].

[7] Energetic internal tides are known to be ubiquitous features of the shelves of Monterey Bay and the California coast. Internal tides in the wider Central California region are often dominated by the semidiurnal M_2 constituent [*Petruncio*, 1993] but diurnal baroclinic motions dominate at some times and locations [*Woodson et al*., 2011]. The intensity of internal tidal motions is controlled, in part, by the degree of stratification [*Petruncio et al*., 1998; *Rosenfeld et al*., 2009; *Wang et al*., 2009]. Offshore in deep waters, energetic low-mode internal tides are generated at the nearby Sur Ridge [*Jachec et al*., 2006] and propagate along the continental margin and into Monterey Canyon. Additional generation, as well as reflection and refraction, may occur both within the canyon and over the Monterey Bay shelf. Within the canyon, internal tides are known to be 10 times more energetic than the open ocean internal wave field [*Kunze et al*., 2002], with amplitudes of 50–120 m and associated flows of 0.2–0.6 m s^{-1} [*Petruncio et al*., 1998; *Rosenfeld et al*., 1999; *Xu et al*., 2002; *Kunze et al*., 2012]. The internal wave field over the shelf can include both onshore and offshore propagation [*Carter et al*., 2005; *Cazenave et al*., 2011] and is characterized by long-wavelength, low-mode semidiurnal waves, as well as high-frequency oscillations characteristic of nonlinear internal bores [*Stanton and Ostrovsky*, 1998; *Key*, 1999; *Storlazzi et al*., 2003; *Cazenave et al*., 2011; *Woodson et al*., 2011; *Walter et al*., 2012].

[8] Over the continental shelf, including the Monterey Bay shelf running northward from the narrow Big Sur coast, sits a band of fine-grained (diameter <63 μm) sediment, predominantly made up of silt and clay-sized particles [*Edwards*, 2002]. This mud belt is composed of material delivered into the coastal ocean from rivers during episodic winter storm events. The Salinas River (Figure 1) has been identified as the source of the mud-belt sediment on the southern Monterey Bay shelf, with highly episodic input driven by winter storms [*Edwards*, 2002]. On average, 90% of the annual precipitation for the Salinas River basin occurs between November and April, during which time discharge rates can exceed 30 m^3 s^{-1}, with corresponding sediment loads greater than 1000 metric tons [*Watson*, 2003]. However, the Salinas River forms a lagoon at the coast, and under nonflooding conditions, the lagoon outflow to the bay is naturally blocked by sand dunes. Only under occasional flood conditions are these dunes removed by the local municipalities, so direct sediment flux to the ocean is rare. Salinas River discharge rates are lowest during late summer and fall months, with a negligible mean discharge rate of <0.2 m^3 s^{-1} for September and October over the years 2000–2013 (U.S. Geological Survey Water Data for California, http://waterdata.usgs.gov/ca/nwis) and zero sediment flux to the ocean. A model of near-bed wave-induced shear stresses for the Monterey Bay shelf region found that under mean conditions southern shelf muds are stable from June through September and start to be mobilized in October [*Storlazzi et al*., 2007]. Despite likely seasonal variations in resuspension, gridded grain size data from two studies conducted in different years show a seemingly consistent quasicircular patch of mud on the southern Monterey Bay shelf [*Edwards*, 2002; *Storlazzi and Reid*, 2010]. This patch appears to be approximately 10–15 km in diameter, centered on the 70–80 m isobaths (Figure 1).

3. Field Experiment and Methods

[9] From 24 September to 27 October 2011, we deployed a wave-driven autonomous vertical profiler, a bottom-mounted, upward-looking acoustic Doppler current profiler (ADCP), and a thermistor chain mooring. All instrument packages were located within 700 m of each other near the 70 m isobath on southern Monterey Bay shelf (Figure 1). The experiment also included a continuous 5 day long series of long-range autonomous underwater vehicle (LRAUV) transects back and forth across the shelf between 12 and 17 October.

3.1. Profiling Mooring

[10] An ODIM Brooke Ocean SeaHorse autonomous profiler was deployed at 70 m depth at 36.7049°N, 121.8700°W (Figure 1). The profiler is wave-powered and uses a ratchet system controlled by an onboard microprocessor to move through the water column. The profiler was instrumented with a SeaBird SBE-19plus CTD, and a Wet Labs WetStar fluorometer and CSTAR transmissometer. These instruments measured, respectively, temperature, salinity, pressure, chlorophyll-a fluorescence, and 650 nm wavelength light beam transmittance (beam attenuation coefficient), all at a rate of 4 Hz. The intake for the flow-through system was located at the top of the profiling package and was controlled by a SeaBird SBE-5T pump. The resting position for the profiler was at the bottom of the cable, 9 m above bottom (mab; at 60 m depth). At the top of every hour, the gripper mechanism released and the profiler floated ($\sim$0.6 m s^{-1}) to the top of the cable 1.5 m below the surface. Upon reaching the top, the gripper mechanism reengaged and winched the profiler back down the line using surface wave energy. Data were collected during the up-casts. The ascent speed of the profiler and instrument sampling rate resulted in a vertical resolution of approximately 15 cm. Over the 5 week deployment period, the profiler collected 847 profiles. In 21 of these the profiler did not winch all the way to bottom of the line before starting a new profile. These were the following: 18:00–21:00 on 1 October, 14:00 and 18:00 on 3 October, 7:00 and 8:00 on 15 October, 11:00–15:00 and 19:00–24:00 on 16 October, 19:00 and 20:00 on 18 October. These incomplete profiles occurred at times when significant wave heights were 1 m or less. The mean starting depth for these shortened profiles was 33.6 m.

[11] Over the 5 week study period, the transmissometer signal became increasingly fouled due to accumulation of

material on the optical windows, and the fouling trend was not linear. We derived corrected beam attenuation values (c^*) by taking each beam attenuation profile and subtracting the minimum c value of that profile from the other profile values. The corrected c^* is thus the degree of beam attenuation above background. Information lost by this correction is the relative difference in background attenuation from profile to profile, and consequently, information about possible whole-shelf and water-column scale changes in background light attenuation. However, since we focus on spatially constrained features and their variability, this was considered an acceptable trade off. The detrending method is similar to that used by *McPhee-Shaw et al*. [2004], where it was applied to cross-margin transects on a per transect basis. In that case, *corrected* values of c were found to have a good linear fit to measured SPM concentrations (filtered and weighed from water-column samples), giving confidence in this approach. At the SPM levels found in the open and coastal ocean, transmissometer beam attenuation coefficient, c, has been found to be linearly proportional to SPM concentration [*Pak and Zaneveld*, 1977]. This has been determined in studies within the nearby Monterey Canyon [*Xu et al*., 2002; *Morrice*, 2011] and also from shelf and slope studies on the northern California margin [*Sherwood and Hibler*, 1994; *McPhee-Shaw et al*., 2004]. We thus assume that c^* and the mass concentration of SPM are proportional and use the two terms interchangeably.

3.2. Acoustic Doppler Current Profiler

[12] A Teledyne RD Instruments 300 kHz WorkHorse Sentinel acoustic Doppler current profiler (ADCP) was deployed in upward-looking mode approximately 670 m north of the profiler (36.7108°N, 121.8688°W; Figure 1) and collected current profiles with 2 m vertical bins every minute. Each ensemble contained 25 pings, with 2.4 s between each ping, and a resulting error (from WinSC planning software) of ± 1.39 cm s^{-1}. The profiles were averaged into 10 min ensembles, reducing the estimated error to $\pm$ 0.44 cm s^{-1}. The ADCP was clamped to a modified structure also used as the base of a vertical thermistor chain. This setup resulted in some data loss due to beam fouling. Of the 34 time gaps due to beam fouling, 21 gaps were $<$2 h in duration, 9 were $<$4 h, 3 were $<$6 h, and 1 gap was 11 h 16 min (on 12 October). In order to preserve the tidal-scale components of the flow, all gaps except the longest one were filled using a spectral method called Joseph's scheme [*Xu et al*., 2002]. A second postprocessing step involved rotating the ADCP's x–y–z components into directional earth coordinates (east-north-up), which was necessary to correct for compass failure. A Nortek acoustic Doppler velocimeter (ADV) was attached to the same frame, so we used the ADV compass readings and the relative orientations of the two instruments' x beams to transform the ADCP data from beam to earth coordinates. The resulting U and V velocity records were also compared to a 4 day long record from an upward-looking RDI 1200 kHz ADCP (W. Shaw and T. Stanton, 2011 unpublished data) located approximately 800 m farther inshore. The bottom 6 bins of 300 kHz ADCP velocities correlated well with those of the 1200 kHz ADCP (mean r was 0.76 and 0.92 for U and V, respectively, with corresponding p values $<<0.005$ for U and V, $n = 468$ for each depth bin). The U and V velocity components were rotated to principle axes, using a $<5°$ rotation. "Along-shore" velocity is essentially north-south, and "across-shore" velocity is east-west, with northward and eastward positive, respectively.

3.3. Thermistor Chain

[13] A vertical chain of 14 SeaBird SBE-39 thermistors measuring temperature every 30 s was attached above the ADCP frame. Thermistors were spaced 5 m apart from 1.5 to 61.5 mab. The bottom, top, and middle (at 1.5, 31.5, and 61.5 mab, respectively) loggers also measured pressure. An Onset HOBO U22-001 temperature logger was also attached to the line at 64.5 mab, and measured temperature every 2 min.

3.4. Long-Range Autonomous Underwater Vehicle Surveys

[14] From 9:30 on 12 October to 20:00 on 17 October the Monterey Bay Aquarium Research Institute's (MBARI) "Tethys" long-range autonomous underwater vehicle (LRAUV) performed continuous 17 km across-shelf transects along a line just to the north of the moorings (Figure 1). The LRAUV profiled in a "yo-yo" pattern from the surface to within 3–5 m above the seafloor, collecting measurements of temperature, salinity, and pressure using a Neil Brown G-CTD, as well as chlorophyll-a concentration and optical volume scattering at 470 and 650 nm using a WET-Labs ECO Puck triplet sensor. The vehicle navigated underwater using a magnetic compass for heading and a Linkquest Doppler Velocity Log for bottom-relative velocity, updated by periodic surface GPS fixes. Each transect was approximately 17 km in horizontal extent and took 5–6 h to complete. The number of profiles completed per km varied with water depth, but on average the LRAUV performed 5 profiles km^{-1}. The profiling pattern was interrupted periodically when the LRAUV surfaced to telemeter data and obtain a GPS position update. Due to uncertainties about the quality of the LRAUV salinity measurements, temperature was used as the basis for comparisons between the physical structure resolved by the profiler and LRAUV data sets. The salinity data from the profiler showed a simple T-S relationship during the LRAUV surveys and no large shifts in salinity, so temperature is considered an adequate representation of the water column physical structure for the purposes of this study.

3.5. Wind, Waves, Tides, and River Discharge

[15] Hourly wind velocity data were obtained from the National Oceanic and Atmospheric Administration's (NOAA) Monterey buoy (Station 46042; www.ndbc.noaa.gov), located 27 nautical miles northwest of Monterey (36.785°N, 122.469°W; Figure 1). Water level height above the mean was determined by applying a band-pass filter (10 h $<$ period, $T < 28$ h) to pressure measurements from the 300 kHz ADCP. Surface wave parameters were taken from the Coastal Data Information Program (CDIP) Monterey Canyon Outer buoy (Buoy 156; cdip.ucsd.edu), located about 9 km offshore from the study site in 170 m of water (36.7608°N, 121.9469°W; Figure 1). The daily-averaged Salinas River discharge rates described in the text were obtained from the U.S. Geological Survey stream gauge located approximately 20 km inland from the coast (Site 11152500, http://waterdata.usgs.gov/nwis).

3.6. Near-Bed Wave Orbital Velocity and Shear Stress

[16] Maximum wave orbital velocity values, u_b, were estimated using the parametric spectral method described by *Wiberg and Sherwood* [2008]. This utilizes standard wave parameters and the Donelan spectral formulation method [*Donelan et al*., 1985] which helps account for times when the wave parameters are inconsistent with a simple, unimodal spectral form. Near-bed shear stresses were estimated from nearest-bed ADCP current velocities and CDIP buoy directional wave measurements using the Grant-Madsen model [*Madsen*, 1994]. In October 2012, a surface sample of seafloor sediment taken at our study site was found to be composed of 95.8% fine-grained sediment with D_{50} and D_{25} of 34 and 14 μm, respectively (C. Storlazzi and K. Rosenberger, 2012 unpublished data). Based on this sample, we used a grain diameter of 34 μm. The model also requires input of an inner hydraulic roughness of the bed, z_o, a parameter which is controlled by several factors including the seafloor material, the degree of small-scale bottom topography (e.g., ripples and biogenic perturbations), as well as flow conditions. Consequently, this roughness parameter is seldom known precisely [e.g., *Cheng et al*., 1999]. We did not directly measure z_o, so we used a hydraulic roughness value of $z_o = 9 \times 10^{-5}$ m, which was a model-tuned estimate used for the soft, muddy portion of the Palos Verdes shelf in southern California [*Ferré et al*., 2010]. *Ferré et al*. [2010] note that this roughness value is lower than those measured for other shelf environments, but is consistent with a seafloor characterized by soft, smooth mud. The critical shear stress threshold, τ_{cr}, for mobilizing noncohesive sediment was calculated using the formulation described by *Soulsby* [1997]. This gave $\tau_{cr} = 0.08$ N m^{-2} for the silt ($D = 34$ μm) sediment at our study site, which matches the critical value used by *Dunbar and Barrett* [2005] to determine the threshold for the resuspension of shelf muds.

4. Results

4.1. Hydrographic and Meteorological Conditions

[17] The full record of meteorological and hydrographic variables is shown in Figure 2. The 5 week study period was characterized by several periods of sustained upwelling-favorable (southwestward) winds, interrupted by weakening or full reversals to downwelling-favorable winds sometimes lasting up to a few days at a time. The two longest duration sustained upwelling-favorable wind events were from 5 to 15 October (with a short 18 h wind relaxation on 11 October) and from 19 to 23 October (Figure 2a). The study period also encompassed several spring-neap tidal cycles (Figure 2b). The first upwelling period coincided with several large surface swell events, while the second was marked by low waves (Figure 2c). During each of the two sustained upwelling-favorable wind events, isotherms and isohalines over the shelf started shoaling about 1 day after wind onset and shoaled progressively, rebounding back to full upwelling and gradually filling the water column from below with cold, high-salinity water (Figures 2d and 2e) throughout the remainder of the event. This, combined with warming surface waters, caused an increase in near-surface stratification, shown (Figure 2f) with the squared Brunt-Väisälä frequency, $N^2 = -g/\rho_o(\Delta\rho/\Delta z)$, where g is the gravitational acceleration, ρ_o is the mean water density of a given profile, ρ is the density at a given depth, z. Under sustained upwelling-favorable winds, subtidal flow was generally alongshore to the south (figure not shown). Within about 36 h of a wind reversal or weakening (such as the wind reversal event seen on 30 September to 1 October and the event of 15–16 October), warmer, lower-salinity water filled the water column from above and stratification over the shelf decreased (Figures 2d–2f). The subtidal flow during these wind shifts was northwestward. These two significant wind reversal events were also associated with an intensification of surface chlorophyll-a extending down to 10–20 m depth at the study site (Figure 2i).

[18] The mean Salinas River discharge rate during our study period was ∼0.9 m^3 s^{-1}, with the largest river discharges (>1.4 m^3 s^{-1}) occurring on 13 October and 26–29 October. While these rates are higher than typical monthly averaged values for September and October (0.2 and 0.1 m^3 s^{-1}, respectively, for years 2000–2010), these rates are still low enough that it is unlikely the lagoon outflow was breached (historically, the sand dunes that block the river outflow are bulldozed by local municipalities only under winter flood conditions). For comparison, the mean discharge for January–May 2011 was ∼34.0 m^3 s^{-1}. Thus, the Salinas River was not a major source of sediment to the bay during the study period.

4.2. Suspended Particulate Features

[19] Numerous SPM features were observed throughout the 5 week study period (Figure 2j). These were found primarily in the bottom portion of the water column, typically at depths >35 m, and were usually not closely associated or colocated with elevated chlorophyll-a fluorescence. An intriguing characteristic of the beam attenuation (SPM) profiles was that, for the majority of profiles, SPM did not increase with depth, as would be expected from a Rouse-like profile, where suspended sediment concentration decreases exponentially with height above the seafloor [*Rouse*, 1937; *Lynch et al*., 1994; *Trowbridge and Nowell*, 1994]. A more typical Rouse profile may exist within a boundary layer closer to the seafloor than we could capture with the profiler's maximum extent of 9 mab. Nevertheless, it is counterintuitive and surprising that many of the strongest SPM signals had maxima centered well above the seafloor (Figure 2j). To identify the location of the SPM maximum in each profile, as well as the vertical extents of near-bottom SPM layers, we first smoothed the c^* profiles vertically using a low-pass filter (Figure 3). Then the minimum profile value was identified, and the algorithm searched for a maximum value below (deeper than) the minimum and with a value of at least 0.5 m^{-1} (c^*). Sometimes maxima were found at the deepest part of the cast (∼20% of all SPM maxima), and we note that in these cases the actual depth of the layer maximum could have been beneath the profiler. The upper extent of the SPM layer was defined as the depth at which the profile intersected a line half way between the minimum and maximum values (Figure 3). When the profiler captured the lower extent of the SPM layer, that bottom limit was found in the same way. Of the 814 hourly profiles, 265 contained identifiable SPM maxima. On average, SPM layers were present

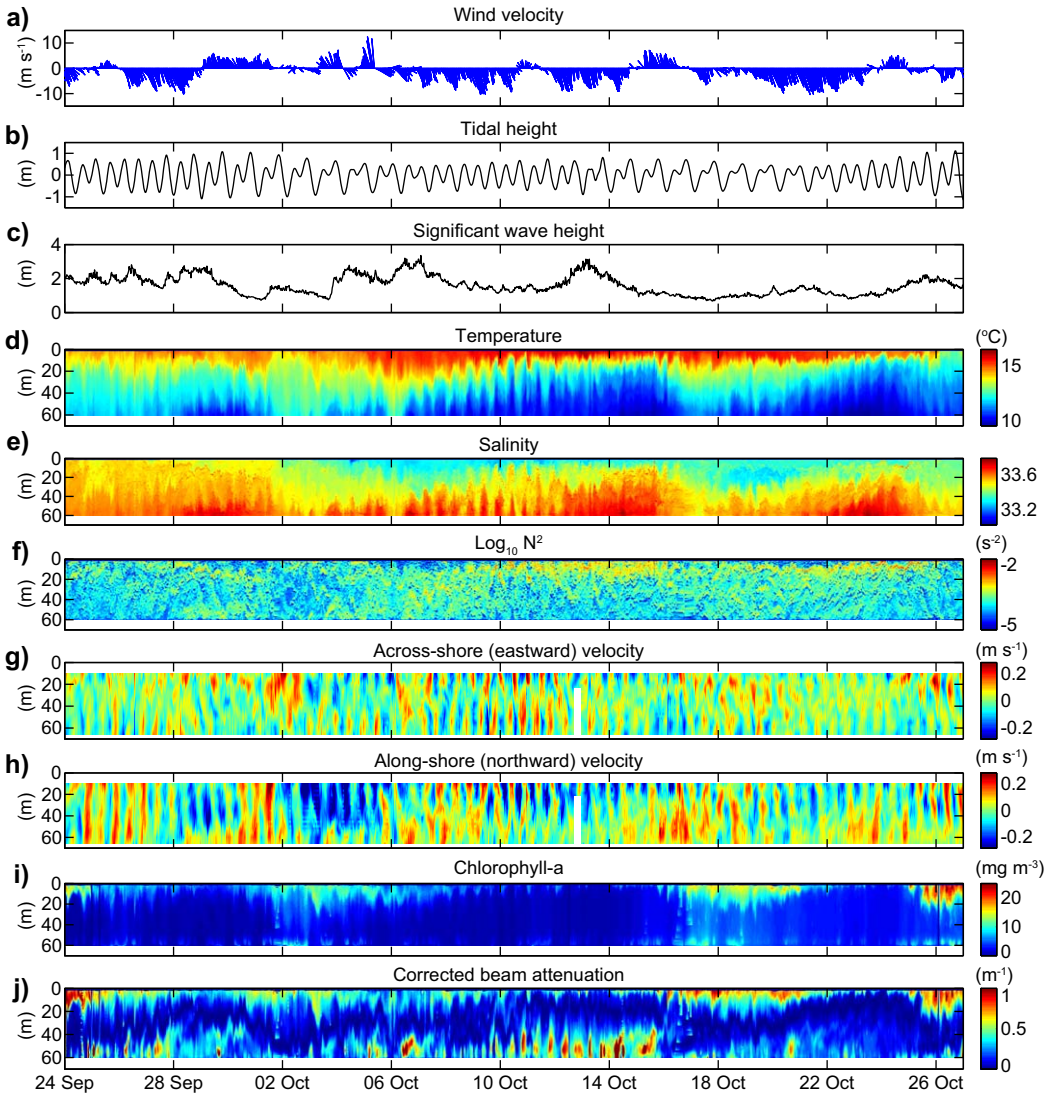

Figure 2. Time series data collected over study period, from 24 September to 27 October, 2011. (a) Wind velocity, (b) water level height above mean, and (c) significant wave height, as well as data from the profiler: (d) temperature, (e) salinity, (f) $\log_{10}$ of the squared Brunt-Väisälä frequency, N^2, (g) across-shore velocity, (h) along-shore velocity, (i) chlorophyll-a concentration, and (j) corrected beam attenuation (c^*). An 11.5 h gap in the current velocity record on 12 October was omitted from the record.

at the profiler site for 4 h at a time. The profiler collected casts down to 9 mab; nevertheless, over 75% of the near-bottom SPM layers had maxima above the bottom of the profile, indicating that, over the measured depth range, the majority of the material was concentrated well above the seafloor. The average height of the c^* maxima was 15.8 mab (51.8 m depth), with the greatest height reaching 33.4 mab. The vertical extent of the SPM layers above the c^* peaks (i.e., the vertical height of the SPM layer) ranged from <3 to 35 m, with an average upward vertical extent of 9 m. To emphasize the midwater column nature of these layers, wherein elevated SPM overlies clear water instead of being found immediately above the seafloor, we will henceforth refer to these features as "detached SPM layers."

4.3. Processes Associated With SPM Features

[20] The detached SPM layers exhibited a great deal of temporal variability. Within the 5 week study period, there were periods of time when SPM features were absent (e.g., 30 September to 2 October and 23–26 October; Figure 2j), followed by periods with numerous SPM events (e.g., 24–26 September and 9–16 October). Some SPM layers appeared as stand-alone events, such as the ones on 6 and 20 October, while others appeared as a series of sequential events separated by mere hours, such as the numerous layers observed between 9 and 16 October. While the detached SPM layers occurred under a wide range of conditions, the majority were observed when winds were upwelling favorable, cold, dense bottom waters were present, and wave heights were >2 m (Figure 2). Why did the SPM layers appear when they did? Were they associated with bottom shear stress and resuspension of sediment from the local seafloor, or were other processes responsible? Which direction was SPM transported during these events? Here we address several mechanisms potentially associated with detached SPM layer formation by contributing either to

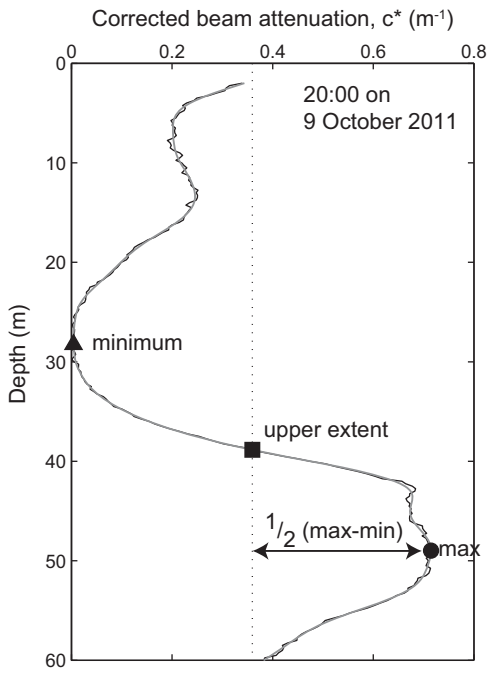

Figure 3. Example profile of a corrected beam attenuation (c^*) profile showing how SPM layer attributes were identified. The light gray line is the smoothed profile, the triangle is the minimum, the circle is the peak, and the square marks the upper extent of the layer. The vertical dotted line indicates the value half way between the minimum and the peak.

sediment resuspension and injection of suspended particulates up into the water column above the seafloor, or to the subsequent transport and dispersal of the suspended particulates.

4.3.1. Bottom Shear Stress From Currents and Waves

[21] First, we examined the relationship between the detached SPM layer events and frictional bottom shear stress due to horizontal near-bed currents and orbital velocities from surface waves (Figure 4) to determine whether the timing of SPM layers was directly related to local sediment resuspension events. Current-driven bottom stress was dominated by tidal-scale variability, likely associated with energetic baroclinic tidal velocities, which are further discussed below. However, current-driven bottom stress alone almost never exceeded resuspension thresholds. Instead, bottom stress associated with surface wave orbital velocities dominated, particularly during several 2–3 day long swell events with significant wave heights over 2 m (28–30 September, 4–7 October, and 13–15 October). Overall, during this 5 week period, combined wave-current shear stresses were above the critical threshold (Figure 4) 30% of the time for grain sizes of $D = 34$ μm. This is consistent with previous descriptions of October as the transition period between the quiescent summer and the energetic winter season, a time when bed shear stresses begin to mobilize seafloor sediment [*Storlazzi et al.*, 2007]. High surface waves resulted in stronger bed shear stresses during the first upwelling period of 6–15 October than during the second persistent upwelling period of 19–23

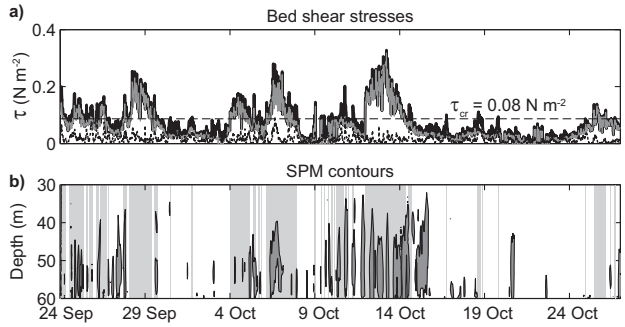

Figure 4. (a) Estimated bed shear stresses for combined wave-current (solid black line), wave-only (gray line), and current-only (black dotted line) stresses. The critical shear stress threshold for grains of diameter 34 μm is overlaid (dashed line; $\tau_{cr} = 0.08$ N m^{-2}). (b) SPM layer contours below 30 m depth, with times when combined wave-current bed shear stresses exceeded critical indicated by the light gray shaded regions.

October. The 6–15 October period was also when the majority of detached SPM layers were observed, suggesting a possible relationship between these features and surface wave-induced bed shear stress at time scales of several days. However, when examined more directly at the event-to-event scale of hours to a day, the relationship is far from clear. SPM features were seen when bed shear stresses were supercritical for the threshold of erosion, but detached SPM layers were also observed when wave heights and bed shear stresses were low, such as during 26–27 September, 14–16 October, and on 20 October (Figure 4b). Furthermore, there was one 2 day period when wave heights and associated bottom shear stresses were high but no SPM features were observed (28–29 September). Generally, since bottom stress was dominated by wave orbital velocity rather than lower-frequency currents, and waves do not vary at the tidal time scales characterizing the primary variance in detached SPM layers, we can infer only an indirect relationship between the timing of sediment resuspension and the timing of these features. The decoupling between local bed shear stresses and detached SPM layers well above the seafloor points to a dominant role of advection in determining the timing of detached SPM layers at this site. While the resuspension of sediment by surface wave action may be a first-order requisite for supplying seafloor material to the water column, once surface wave-induced resuspension occurs, other processes such as near-bottom currents appear to then determine how and where this material is transported.

4.3.2. Energetic Internal Tides

[22] The SPM and current patterns observed during the week of 9–16 October suggest a strong relationship between detached SPM layers and onshore transport at tidal time scales. Near-bottom currents and isotherms both exhibited strong fluctuations at the semidiurnal frequency (Figures 5a and 5b). This periodicity was especially strong in the across-shore (east-west) current component. To show the temporal variability of the semidiurnal velocity variance, we used the Morlet nonorthogonal wavelet function

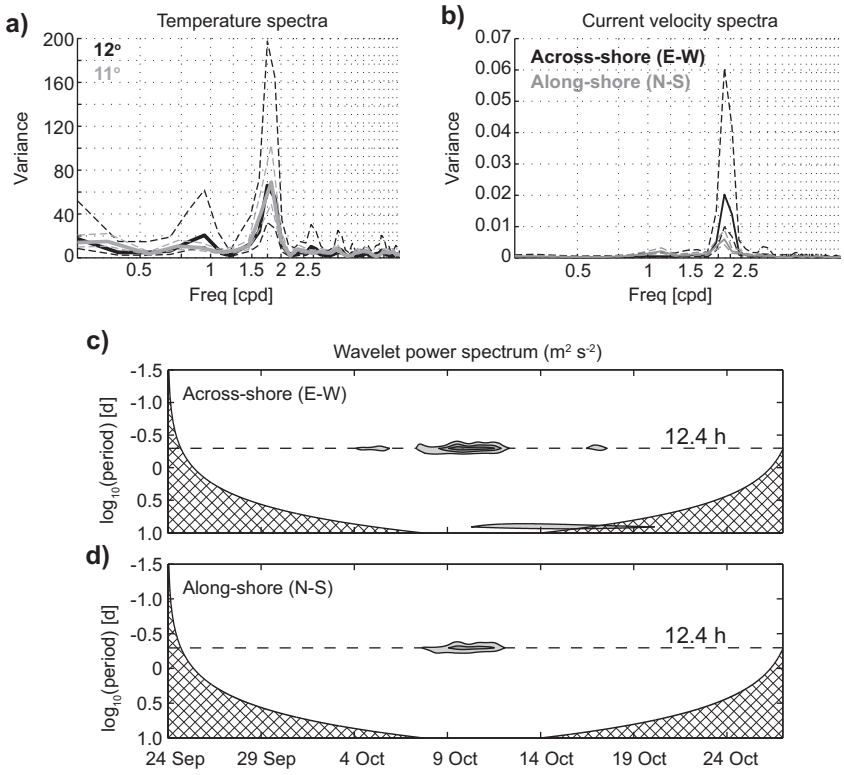

Figure 5. Variance-preserving energy spectra of (a) near-bed isotherms and (b) velocity components from 16 mab, with the dashed lines indicating the 95% confidence interval for each spectrum. Also, a wavelet power spectrum [*Torrence and Compo*, 1998] for (c) across-shore and (d) along-shore velocity at 16 mab for the entire time series; the parabolic black line indicates the "cone of influence"; in the hatched region below this line errors due to edge effects become significant. The shading levels indicate 25% (lightest gray), 50%, and 75% (darkest gray) of maximum energy.

method outlined by *Torrence and Compo* [1998] to compute the wavelet energy spectrum of the across-shore and along-shore current velocities at 16 mab (53 m depth; Figures 5c and 5d). Energy at the semidiurnal frequency in near-bottom temperature and currents peaked between the period of 9–11 October (Figures 5c and 5d). This period of elevated internal tidal kinetic and potential energy coincided with the start of the week-long period (9–16 October) of particularly intense and repetitive detached SPM layers (Figures 2j and 6).

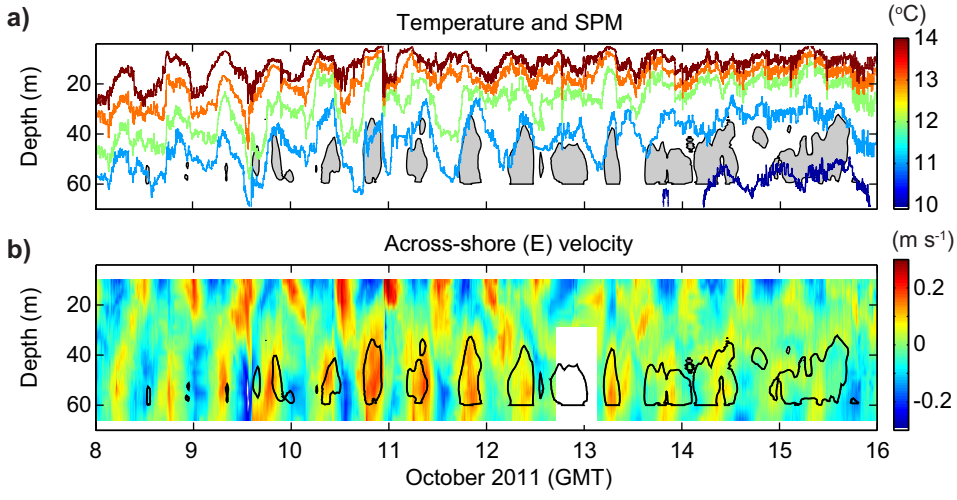

Figure 6. Subset time series for the time period of 8–16 October showing (a) temperature contours at 1°C steps (from 10 to 14°C) from the thermistor chain with SPM contours (gray shading) overlaid, (b) across-shore velocity with SPM contours (thick black contours) overlaid.

[23] Detached SPM layers during this week-long event (which also coincided with an upwelling period, as discussed above) were characterized by a clear relationship between SPM and the onshore movement of water during the onshore (at bottom) phase of the semidiurnal internal tide. This is seen in Figure 6, where the depth and time range of SPM layers are shaded in gray and can be seen to be tied to the arrival of cold water and, for the most part, closely match the time and depth span of the onshore component of across-shore velocity.

[24] A series of sequential profiles show the development of near-bottom onshore flow and the associated thermal structure and SPM profiles during an example semidiurnal period on 10 October (Figure 7). Currents were characterized by a two-layer, vertical mode-1 structured flow. The upper water column flowed obliquely onshore and offshore (southeastward and northwestward) with falling and rising isopycnals, respectively, while the lower half of the water column flowed weakly along-shore (southward) during falling isopycnals and strongly onshore (eastward) with rising isopycnals. The SPM maxima were roughly associated with the peak in near-bottom, onshore flow (Figures 6b and 7). Again we call attention to the fact that SPM maxima were located well above the bottom of the profiler cast, overriding clearer water closer to the seafloor.

4.3.3. A Vertical Updraft Event

[25] On 9 October from approximately 12:00 to 14:00, a large-amplitude internal wave of depression passed the study site and caused the pycnocline (~13°C isotherm) to deepen 14 m in 30 min (Figure 8a). Below the descending isotherms, offshore-directed bottom currents were vigorous, at >0.3 m s^{-1}. This isopycnal depression was then immediately followed by abrupt shoaling; the 11°C isotherm jumped from deeper than 70 up to 56 m depth in <4 min. The vertical adjustment coincided with a sudden reversal in bottom currents from offshore to onshore. The Froude number, a dimensionless value used to characterize a flow's resistance to gravitational effects, was calculated as $Fr=|u/c|$, where u is the current speed at a given depth and c is the first baroclinic mode phase speed, approximated as $c=1/\pi \int_{-H}^{0} N(z)dz$ [*Chelton et al.*, 1998]. *Fr* calculated using the combined thermistor mooring and ADCP data (Figure 8b) demonstrate unstable conditions associated with the strong bottom currents (supercritically surpassing the baroclinic phase speed) compressed into a small space, and increased stratification from isopycnal sinking and compression. These results are suggestive of an internal hydraulic jump or strongly nonlinear conditions. Isopycnal ascent of over 14 m in 4 min implies vertical velocities of >0.06 m s^{-1}, and such vertical velocities were confirmed directly by the 2 min ensemble (nonaveraged) ADCP measurements. Positive vertical velocities during the initial jump reached 0.068 m s^{-1}, with a second peak in vertical velocity of 0.048 m s^{-1} approximately 10 min later, and a downward velocity between these peaks of only −0.024 m s^{-1} (Figure 8c).

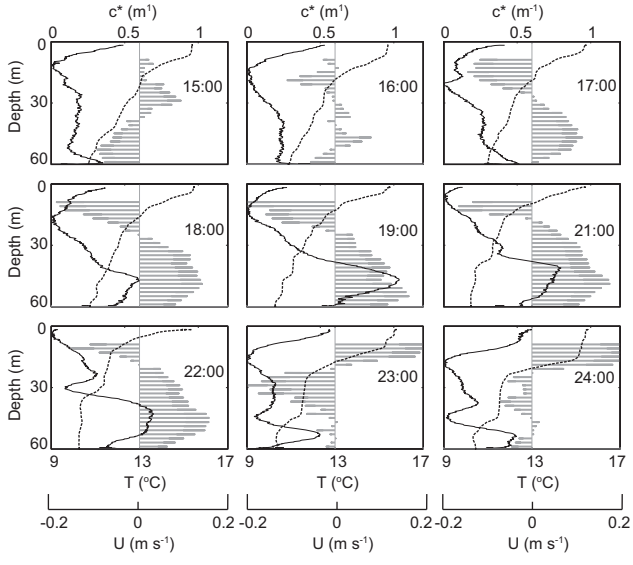

Figure 7. Series of profiler casts and across-isobath current profiles from 15:00 on 10 October to 00:00 on 11 October (GMT). Black line is corrected beam attenuation (c^*), dotted line is temperature, and gray bars are across-shore velocity (U). Time of each profile is indicated on right-hand side plots.

[26] Such vertical velocities are capable of lifting suspended particulates substantial distances from the seafloor up into the water column. The Stokes settling velocity ($w_s=\left[g(\rho_s-\rho_f)/18\mu\right]D^2$, where ρ_s and ρ_f are the respective sediment and fluid densities, μ is the dynamic viscosity of seawater, and D is the particle diameter) for the median size class of observed sediments (D_{50} = 34 μm) is $w_s = 7 \times 10^{-4}$ m s^{-1}. Given the flocculation ability of this sediment size class [*van Leussen*, 1999], the true settling velocity of these particles in aggregates could be up to an order of magnitude larger, ~4×10^{-3} m s^{-1} [*Sternberg et al.*, 1999]. Nonetheless, taking the aggregate and the Stokes settling velocities as approximate upper and lower limits still gives a range of settling velocities 1 to 2 orders of magnitude weaker than the peak vertical velocity during the 9 October event. An upsweep event with a net velocity ($w - w_s$) of 0.04–0.06 m s^{-1} would lift aggregated fine-grained sediment to a height of 21–34 mab within 10 min. We note that in these calculations we assumed a vertical, not diapycnal, reference frame. The vertical advection observed during such events could very well be strongly along-isopycnal, given the intense tilting seen at the same time in the thermistor mooring record (Figure 8a). The implication is that such updraft events could play an important role in the formation of the detached SPM layers whose center of mass was on average 16 mab but was observed as far up as 33 mab. We will return to this in section 5.

4.4. LRAUV Transects

[27] Although LRAUV transects did not span a long enough period of time to allow a before-and-after look at events surrounding the 9–16 October episode of repeated detached SPM layers, they did overlap with the latter portion of the week of interest, from 12 to 16 October. The frequency of the LRAUV transects was too sparse for these data to be useful for examining events occurring at subdiurnal time scales, such as the energetic internal tides and updraft event described above that were strongly linked to the detached SPM layers observed by the profiler.

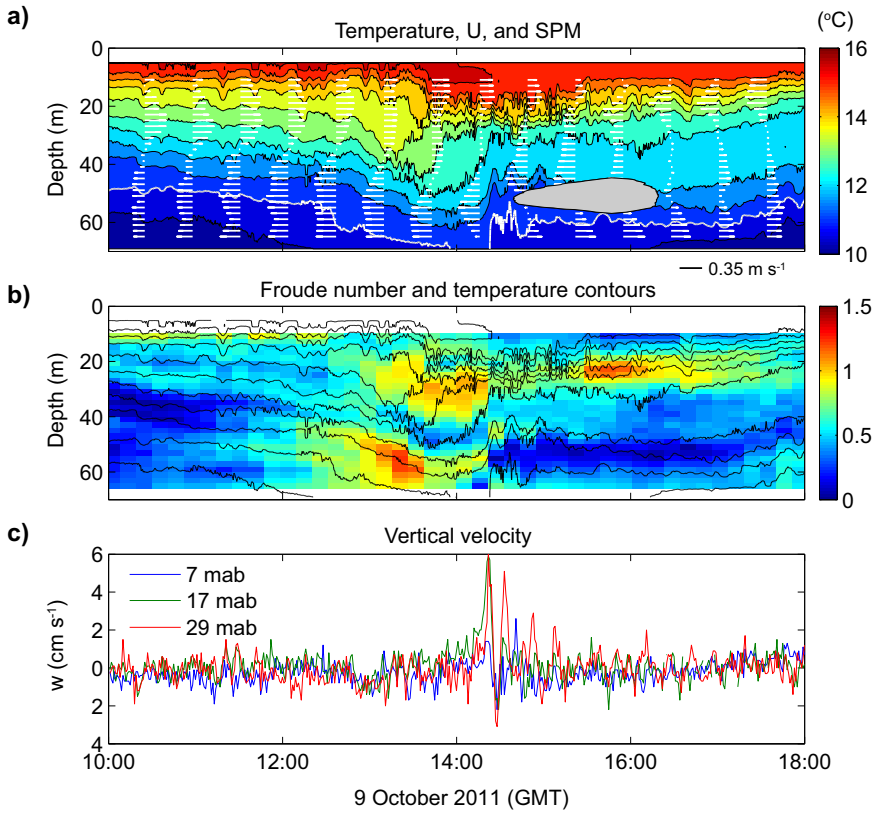

Figure 8. An 8 h time series from 9 October. (a) Temperature contours, onshore (east-west) current profiles (white horizontal lines), and SPM features (gray patch); the thick white contour marks the 11°C isotherm. (b) Froude number with temperature contours from Figure 8a overlaid; yellow to red colors indicate regions of critical or supercritical flow. (c) Vertical velocity from the 2 min current measurements at 7 (blue), 17 (green), and 29 (red) mab.

Nonetheless, the across-shelf LRAUV transects provide unique spatial information about the hydrography and SPM patterns over the shelf. During the 5 days of across-shelf transects, the LRAUV performed 19 yo-yo profiling runs, of which 11 are shown in Figure 9, and SPM features, either near-bottom or detached, were found in all but one of the transects. These features were observed at all shelf depths covered by the LRAUV, and ranged in thickness from several to 10s of m. Most of the SPM features resolved in the across-shelf transects appeared to be BNLs, or "bottom-attached SPM layers" (to distinguish them from the detached SPM layers seen by the profiler). Some of these features were quite thick, sometimes as thick as 20–30 m (e.g., Figures 9e–9i). SPM patterns across the shelf could change dramatically over the course of one or two transects. On the first 13 October transect, thin patches of SPM were found at a few spots over the shelf (Figure 9c); 24 h later, during the first 14 October transect, a large SPM layer that extended nearly 30 mab was present between the 80 and 60 m isobath (Figure 9e). This occurred roughly one day into a high wave event with intensely elevated bottom shear stresses starting on 13 October (Figures 2c and 4a).

[28] Near-bottom SPM layers seemed to be more common than detached SPM layers in the LRAUV data. However, there were several observations of detached SPM layers, in the form of intrusions suggestive of offshore-spreading INLs (Figures 9g–9i), as well as detached layers of SPM overlying clearer water, which may have been dispersing in both the offshore and onshore direction (Figure 9i). These detached features (some of which may have been in the process of detaching) were all found between the 10 and 11°C isotherms.

5. Discussion

[29] Although surface wave and current-induced bed shear stresses surpassing erosion thresholds at 70 m depth may have increased the general likelihood of suspended particulates in the water column, bottom shear stress was not a direct predictor of the detached SPM layers that dominated suspended sediment and transport events above 9 mab during the 5 week long experiment. Elevated bed shear stresses may "set the stage" for these SPM events by providing sufficient energy to keep the bottom boundary layer immediately above the seafloor filled with suspended particulates. Assuming near-bed currents of similar magnitude to those we observed at 70 m, moderate surface waves (significant wave heights >2 m, peak wave periods >10 s) can produce combined wave-current bed shear stresses that exceed critical ($\tau_{cr} = 0.08$ N m^{-2}) at shelf depths as deep as 100 m. This near-bottom water could then be a steady source for the elevated particulates seen in the detached layers higher up in the water column. This interpretation is

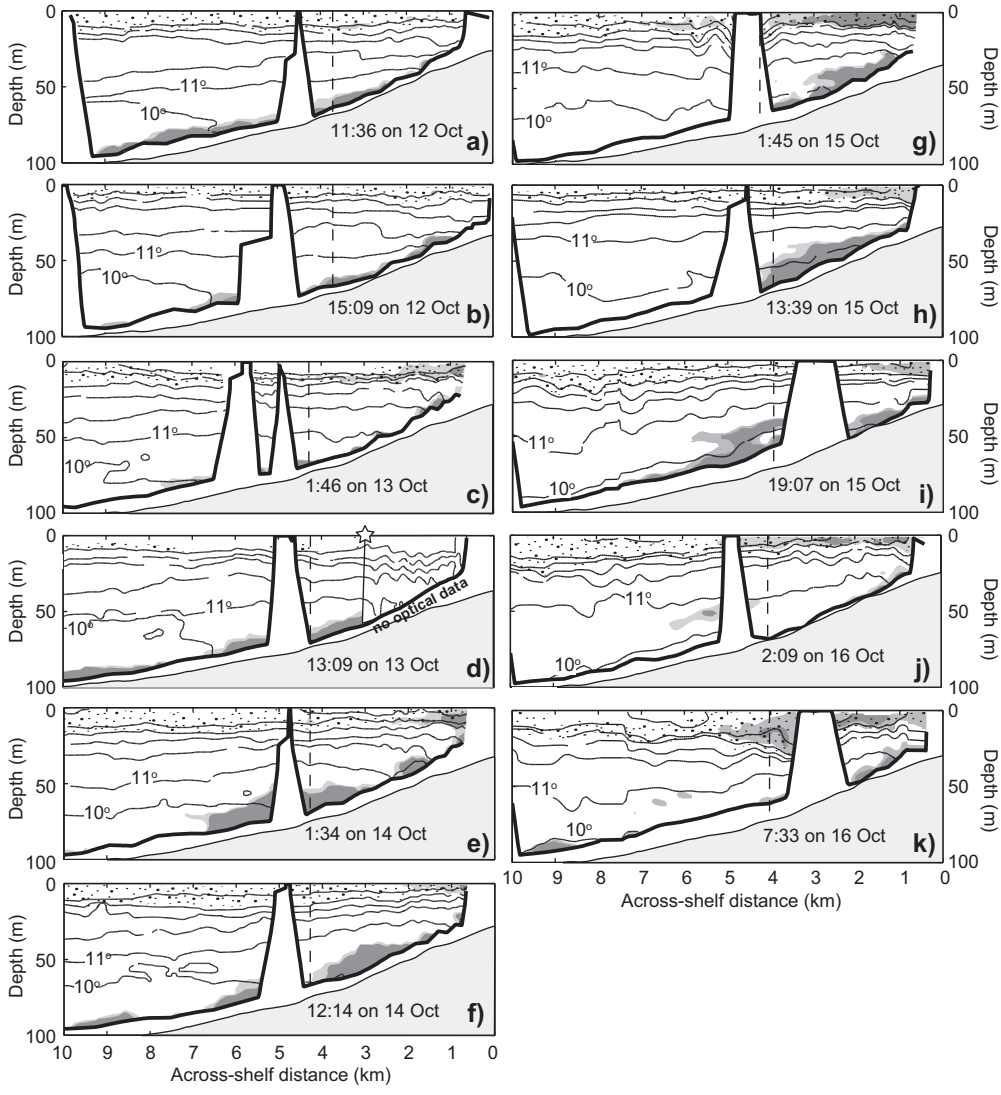

Figure 9. Long-range autonomous underwater vehicle (LRAUV) transects from 09:30 on 12 October to 20:50 on 16 October. Plots are oriented offshore to onshore (west-to-east). *X* axis is across-shelf distance from a common longitude marking the most eastward extent of the combined transects. Thin black contours are isotherms (1°C steps), light gray shaded areas are volume scattering $>1.5 \times 10^{-3}$ m^{-1}, and dark gray shaded areas are volume scattering $>2.5 \times 10^{-3}$ m^{-1}. Stippled regions indicate where chlorophyll concentrations were >2 mg m^{-3}. The thick black line marks the bottom extent of LRAUV yo-yo's and the area with light gray shading below this is the approximate seafloor depth. Note: the LRAUV normally reached depth 3–5 mab, however at the midpoint of each transect the vehicle surfaced to telemeter data and obtain a GPS fix, and the trapezoidal pattern in the thick black line reflects this deviation from profile collecting. In (d), both the optical backscatter and chlorophyll fluorescence measurements were fouled inshore of the line marked by the star, so these values were omitted.

consistent with the across-shelf snapshots provided by the LRAUV, which show an increase in near-bottom SPM features during the period of 13–15 October, when surface wave heights and associated bottom shear stresses increased (Figures 2c, 4, and 9d–9g). The detached SPM layers observed by the profiler also show these features lengthening in duration during this time period.

5.1. Vertical SPM Distribution

[30] Detached SPM layers centered well above the seafloor (16 mab on average) dominated suspended particulate transport within the depth range measured with the automated profiling mooring (9 mab to 1.5 m below surface). These layers were on average centered 16 mab, but maxima were seen as high as 33 mab. The detached SPM layers were on average 9 m thick in the vertical. This is thicker than whatever bottom nepheloid layers may have existed, since we did not usually see BNLs extending up into the bottom portions of the profiler record, >9 mab. Elevated SPM concentrations over such extensive vertical scales suggest that a significant contribution to shelf suspended sediment transport may occur within these detached SPM layers.

[31] There are several possible explanations for why SPM profiles so often had peaks above the seafloor overlying clearer water instead of SPM continuously increasing with depth. One possibility is that particulates are lifted into the 10–30 mab range by strong vertical updraft events (e.g., Figure 8) as discussed above, but then the above-bed SPM peaks are focused by sheared lateral advection. Baroclinic currents were weakest closer to the seafloor and generally peaked at the same depth where the SPM peaks were observed (Figure 7). This interpretation is similar to that of *Inall* [2009], who examined upslope movement of detached boundary dye intrusions and noted that the maximum dye concentration should be expected to be above the bottom in the upslope direction since the upslope velocity must tend to zero at the bed.

[32] Another possibility is that isopycnals associated with an initial uplift event, and thus with elevated SPM, flatten out as the leading face of the bore upsurge collapses (Figure 10). This could help distribute SPM along-isopycnal in both the offshore and onshore directions. Near-bed SPM features have been observed on the Oregon shelf [*Klymak and Moum*, 2003] as well as near the shelf break in southern Monterey Bay [*Carter et al*., 2005]; in both cases, the SPM patterns were associated with nonlinear internal waves (NLIWs) that appeared to have trapped cores, a wave feature that arises when water velocities exceed NLIW propagation speed, and also show above-bed maxima with clearer water within the core. It is also possible that the observed SPM profiles arose from vertical convergent fluxes within a profile of depth-varying vertical diffusivity. *Brun-Cottan et al*. [2000] demonstrated numerically how a "puff" of resuspended seafloor material originating from a vertical injection of sediment into the water column would produce a concentration profile with a peak well above the seafloor that resulted not from baroclinic currents but from simple BBL shear. Matching our suggestion that the majority of the observed SPM layers were generated deeper on the shelf, in *Brun-Cottan et al*. [2000] simulations, the above-bed SPM peaks only appear some distance away from the injection point.

[33] In contrast to the detached SPM layers observed at the mooring site, the majority of SPM features captured in the across-shelf LRAUV transects appear to have been closer to seafloor (Figure 9). This likely reflects the different spatial and temporal scales captured by the two instrument platforms. As mentioned before, the majority of LRAUV transects took approximately 12 h to complete, thus not only spatially aliasing any patterns moving across-shelf, but also temporally aliasing any dynamics happening at, or below, semidiurnal time scales. The duration of each layer at the profiler was, on average, 4 h, and these layers were associated with processes such as internal tides and nonlinear isotherm adjustments, which occurred at a semidiurnal period or less. That said, the LRAVU transects give rise to many remaining questions about the relationship between the detached and near-bottom SPM layers. Do the BNLs seen in the across-shelf transects serve as a source for the onshore-moving detached SPM layers seen by the profiler? And is this near-bottom SPM controlled primarily by surface wave stresses on the seafloor, or does injection of seafloor material by nonlinear baroclinic motions also contribute? This study provides guidance for future investigations with autonomous underwater vehicles (AUVs). For example, setting a higher flight angle but constraining the yo-yo pattern to the bottom half of the water column might achieve better horizontal resolution of, say, <100 m, to capture the detached SPM features. AUV paths might be designed to track the along-shelf extent of these features or to follow them in a Lagrangian "feature-capture" mode. In addition, the comparison of the data sets from the moored

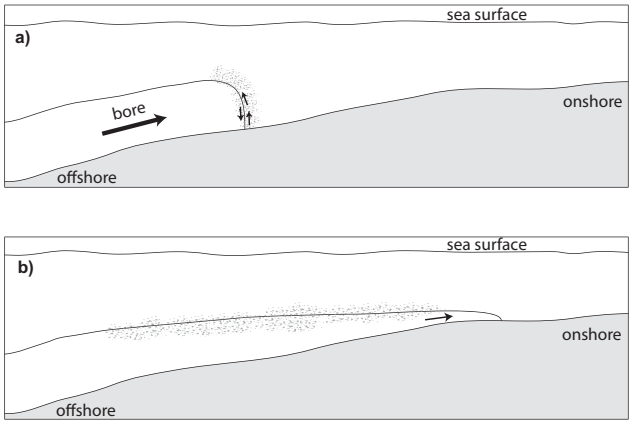

Figure 10. Conceptual schematic showing one possible mechanism for producing the observed above-bed SPM layers: (a) the upslope surge of a bottom internal bore with sharp leading edge causes updraft of seafloor sediment (stippled shading), and (b) the subsequent collapse and flattening of this front holds the suspended material in a layer above the seafloor as it disperses laterally along isopycnals.

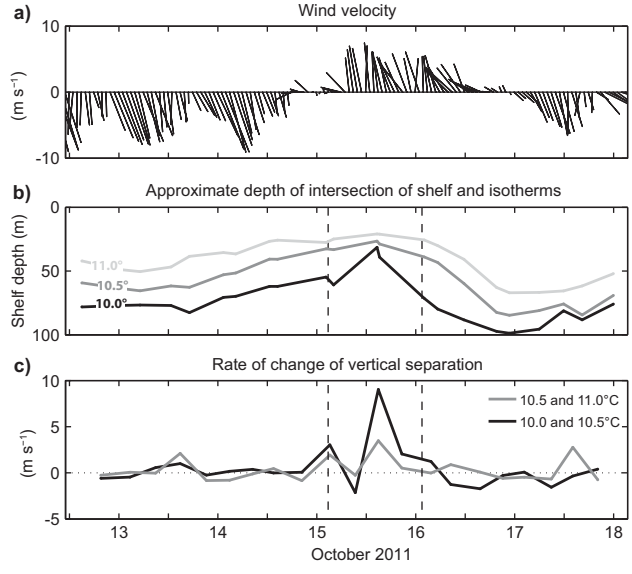

Figure 11. A 5 day time series from 13 to 18 October 2011 showing wind forcing and related changes in across-shelf hydrography as measured by the long-range autonomous underwater vehicle (LRAUV). (a) NOAA-buoy wind velocity showing magnitude and heading direction. (b) Approximate isobath where 10.0, 10.5, and 11.0°C isotherms intersect the shelf. (c) Rate of across-shelf vertical spreading between the isotherms shown in (b).

and moving instrument platforms underscores the challenges of adequately resolving SPM transport across multiple spatial and temporal scales. SPM observations will need to achieve a repeat time of at least 6 h (the Nyquist period) to capture these semidiurnal upslope transport patterns.

5.2. Origin, Transport, and Fate of Detached SPM Layers on the Shelf

[34] The association between SPM and onshore-moving colder waters does not necessitate a direct relationship between SPM and 10–12°C waters. Although not shown, analyses of regression between temperature-salinity properties and SPM, both throughout the entire record as well as within the shorter 9–16 October period, found no water-mass-to-SPM relationship. In addition, if there had been a close relationship we would have seen elevated SPM not only during the upswing (shoaling isotherms and onshore near-bottom flow) phase of the internal tide, but also during the falling (deepening isotherms and offshore or downslope near-bottom flow) phase of the internal tidal currents, after the coldest waters started to turn around and move back downslope. Instead, throughout 9–14 October, detached SPM layers appeared at the mooring only during onshore currents. Then, between 14 and 16 October, the relationship between SPM layers and onshore transport became less clear. This may be due to the increase in wave-induced bed shear stresses during this period. Internal tides were weaker, yet the detached SPM layers were present and occurred over longer durations, possibly indicating that these layers had a greater horizontal spatial extent during this period, or that there was simply a greater amount of SPM within the BBL due to surface wave resuspension.

[35] The updraft event on 9 October (Figure 8) occurred just 17 min before the first in the 9–16 October series of SPM layers, whose maximum was centered 17 mab, was seen at the mooring site. For this SPM layer, we have shown that the vertical velocities during the updraft event could easily have lifted suspended particulates (both individual and flocs) up to at least 17 mab within this time frame. We tracked a theoretical particle at the depth of this SPM peak backward in time using progressive vectors from the three-dimensional ADCP velocities. We assigned this "particle" a range of sinking velocities, from the Stokes sinking velocity for 34 μm particles (7×10^{-4} m s^{-1}) to the estimated sinking velocity for large flocs (4×10^{-3} m s^{-1}) [*Sternberg et al*., 1999]. These calculations put the initial generation site within 200 m of the profiler for disaggregated particles, and within 500 m of the profiler for aggregates. This implies that such a vertical pulse, followed by across-shelf transport in the bottom layer of the mode-1 internal tide, is a plausible conceptual model for the formation and transport of these features. The idea that intense and coherent vertical velocity events, such as the "updraft" event described here, could cause convective transport of SPM on a regular basis represents a new possible pathway by which sediment and other seafloor material is transported over the shelf. Most observational studies have focused on transport within the BBL. Here instead, we propose a mechanism that might routinely discharge BBL fluid, along with its load of elevated SPM, up into the middle reaches of the shelf water column. This could be an important factor in setting the circumstances leading both to offshore SPM transport in intrusions (detached INLs) and to onshore transport within detached SPM features such as those described here.

[36] The updraft event itself appears to have been an abrupt isopycnal adjustment, associated with either a hydraulic jump or a nonlinear internal bore, characterized by rapid deepening of the middle layers of the water column and compression of intense currents into a thin layer above the bottom. NLIWs and hydraulic jumps have been observed to occur on continental shelves immediately after critical Froude conditions [*Holloway*, 1987; *Xu et al*., 2011], and, indeed, on 9 October supercritical *Fr* values were attained near the seafloor just before the observed vertical updraft event (Figure 8). The larger scale isopycnal descent before the abrupt transitional jump was itself set by the longer wavelength semidiurnal internal tide, but included straining and vertical divergences caused by the 11.0–12.0°C isotherms descending while the upper 12.5–13.5°C isotherms simultaneously ascended (Figure 8a). Alternatively, this updraft event may have been caused by the sharp leading edge of NLIW or bore. In either interpretation, the updraft event was associated with both linear internal tides (the initial descending isotherms) and with nonlinear features of internal waves (the abrupt vertical displacement of isopycnals; Figure 8).

[37] Others have reported similar upsweeps of fine-grained seafloor particles along severely tilted isopycnals at the abrupt edge of NLIWs on mid or outer continental shelves [*Bogucki et al*., 1997; *Johnson et al*., 2001; *Klymak and Moum*, 2003; *Moum et al*., 2007]. Of particular relevance are observations from very near our study site, on the southern Monterey Bay shelf in water depths of 70–90 m, where *Carter et al*. [2005] noted acoustic backscatter pulses extending upward from the seafloor to between 20 and 50 mab. The authors suggested that these features were caused by steep nonlinear adjustments associated with *offshore*-propagating NLIWs. Although their 120 kHz acoustic scattering observations were of much larger particles than those described here, the upsweep mechanism for particle injection would work for both categories of particles; during time scales of 10 of min, neither large nor fine particles would have the chance to settle very far.

[38] While we cannot know the exact timing of the 9 October SPM layer in relation to the updraft event, since the SPM profiles were taken hourly, the particle-tracking model suggests that this first detached SPM layer of the 9–16 October series was generated locally. Subsequent SPM layers, however, appear to have been initiated further upstream, somewhere deeper on the slope. We argue this for several reasons. First, for the remainder of the 9–16 October period, no further updraft events were observed at the site. Second, alternating onshore-offshore velocities in the bottom portion of the water column, characterized by mode-1 (or two-layered) semidiurnal internal tides, were the dominant currents advecting the detached SPM layers. Once in suspension, particles of $D = 34$ μm would take approximately 6–8 h to sink back down to the seafloor from a height of 15–20 m, while aggregated flocs ($D \sim 250$ μm) would settle out within 1–2 h. Assuming the SPM was not entirely composed of flocculated material, it is probable that the detached SPM layers were often seen at the

mooring at least several hours after their initial injection into the water column. Given the near-bottom current speeds and these settling time scales, we estimate that the SPM in these subsequent layers originated from 0.5 to 1.5 km downslope from our study site. However, we note that smaller particles, such as the 14 μm size category (D_{25}) that were also observed at our study site and to which transmissometers also respond well, could persist in suspension over multiple back-and-forth tidal excursions.

5.3. Repeated SPM Injection Events and Net Onshore Transport

[39] The above scaling arguments for particle settling combined with advective transport suggest that individual detached SPM layers during the 9–16 October series were regenerated on each semidiurnal tidal cycle. An alternative possibility for the 9–16 October series of SPM events is that one initial event injected particles into the water column and that these particles then remained at their initial isopycnal to be advected back and forth past the mooring site within multiple internal tidal excursions until laterally dispersed and diluted, or until shelf waters were replaced by another water mass. The duration of individual detached SPM layers increased from about 2 to 11 h over the course of the 9–16 October period. Based on a mean onshore current of 0.15 m s^{-1} advecting an SPM layer patch past the mooring each time it was seen, this expansion in time would predict a horizontal patch size spreading from about 0.5 out to 7.0 km. A simple scaling for estimating lateral diffusivity ($K_H \sim L^2/T$, with $T = 7$ days and $L = 4000$ m) gives $K_H = 20$ m^2 s^{-1}. However, this interpretation is incompatible with observed net along-coast currents of 0.05–0.10 m s^{-1}, which would transport waters approximately 30–60 km over 7 days, demonstrating the unlikelihood of a water mass occupying the shelf long enough to undergo back-and-forth tidal advection around the study site for an entire week. SPM maxima also changed position slightly in isopycnal space from one event to the next, which is also incompatible with model of advection of a single patch.

[40] For these reasons, we argue that during the 9–16 October series of detached SPM layers, SPM injection likely reoccurred on or before the upslope phase of every semidiurnal tide. This would introduce new material to the water column approximately every 12 h, as long as the appropriate stratification and internal tidal energetics conditions held favorable for both injection and transport, and there was an ample supply of suspended material within the bottom boundary layer. This latter condition likely necessitates fairly energetic surface waves (approximately >2 m significant wave height) within just a day or two of the events.

5.4. Implications for Continental Shelf Mud Belts

[41] An important implication of the "repeated injection events" model is that it would result in a substantial onshore flux of sediment from outer to midshelf depths. We suggest a conceptual model whereby approximately every 12 h, during a period of favorable conditions, seafloor sediment on the outer shelf was rapidly kicked up into the mid-depth water column well above the BBL, whence it was then advected several kilometers onshore, and, subsequently, settled back to the BBL or seafloor. This could represent an important expansion of our understanding of how midshelf mud belts are built up and sustained. The more commonly understood pathway is for sediment to be resuspended by surface waves at shallower depths, followed by net migration offshore to the midshelf. Here we suggest an additional pathway where erosion and resuspension occur deeper on the outer shelf and are followed by shoreward transport toward the middle and shallow sections of the mud belt. Shoreward transport of SPM was recently demonstrated in numerical simulations by *Bourgault et al*. [2013], whereby long internal solitary waves breaking on a uniform shelf resuspended fine-grained sediment that was subsequently transported shoreward in the form of boluses. Frequent onshore transport of what may be "boluses" of suspended material within the cold, dense water right near the front of an up-surging NLIW could also lead to enhanced across-shelf flux of SPM due to an intensification of lateral gradients. The intense lateral gradients formed during upslope-surging nonlinear internal tides have been shown to cause a net flux of heat away from [*Nam and Send*, 2011] and nitrate toward [*Lucas et al*., 2011] the inner shelf in the Southern California Bight. Similar dynamics could apply here, where the pushing of sediment laden water upslope into clearer (less turbid) water, and consequent intense SPM gradients across the front, could cause net shoreward transport of fine material.

[42] Revealing the pathways by which fine-grained material is dispersed over the shelf is critical for understanding how and to what degree midshelf mud belts drive biological processes in the coastal environment. The problem is complex because, as noted by *Palanques and Biscay* [1992], the distribution of mud material on the shelf is often decoupled from the patterns of SPM in the overlying water column. The cross-shelf SPM patterns we observed in the LRAUV transects are another example of this (Figure 9). In addition to delivery of nutrients, trace metals, and organic material to the euphotic zone, there is evidence that the shelf generation sites and transport patterns of SPM are important determinants in the diversity and density of benthic organisms on the shelf, possibly even more so than the shelf substrate type [*Puig et al*., 2001; *Oliver et al*., 2011].

5.5. Wind-Driven Upwelling, Internal Tides, and SPM Events

[43] A final important finding of this study is that favorable conditions for detached SPM layers on the Monterey midshelf appear to include not only large enough surface waves for recent seafloor resuspension in the BBL but also, and of equal importance, energetic internal tides. Under mean summer hydrographic conditions, the southern Monterey Bay shelf is critical to the M2 internal tide at the shelf break, as well as directly upslope from the inshore mud belt boundary (~30–50 m isobaths) [*Jachec*, 2012]; however, the inshore critical slope region likely varies depending on regional hydrography and stratification. It is important to note that during our study the internal tide exhibited low-frequency variability that was decoupled from the surface barotropic tidal energy. *Nash et al*. [2012] note that internal tides along continental margins are intractably intertwined

with a complex interplay of multiple remote mesoscale and submesoscale processes, making an explanation of the variable strength of the observed internal tide on the shelf extremely difficult, if not impossible. Though we cannot predict the timing of strong internal tide forcing, the ability of energetic internal tides to propagate into Monterey Bay appears to also be set by wind-driven shifts in stratification over the shelf. During our 5 week study, the influx of dense water up onto the shelf provided the stratification necessary to support energetic two-layered internal tides. Such intense internal motions could not exist at the depth range of the study site when the shelf water column was less stratified and filled with warmer water, such as was seen after a few days of downwelling-favorable winds (e.g., 2–4 October; Figures 2d, 2e, 2g, and 2h). We suggest that at this shelf depth, wind-driven variations in bulk hydrographic conditions over the shelf may be just as important for sediment transport events as the more commonly considered surface swell events that erode the seafloor.

[44] In addition, upwelling-relaxation dynamics may also directly drive some of the SPM patterns over the shelf, due to the unbalanced responses of the across-shelf density structure to wind shifts. Using a numerical simulation, *Austin and Lentz* [2002] found an unbalanced response in across-shelf transport under upwelling and relaxation conditions, and they noted that the depth of the pycnocline may determine the time scales of these responses. In the across-shelf LRAUV transects, we observed evidence of convergence and divergence in the shelf isotherms coinciding with the development and detachment of an INL near the 40 m isobath. The transect series from 15 to 16 October show an SPM layer between the 10.0 and 11.0°C isotherms detaching from the continental shelf and spreading seaward (Figures 9g– 9j). A distinct lift-off of the layer was captured at approximately 2:20 on 15 October (Figure 9g) at a depth of about 40 m. Clear water can be seen beneath the feature. A strong convergence between the 10.0 and 10.5°C isotherms occurred between this transect and the one prior (Figure 11c); this convergence was caused by a run-up of the 10.0°C isotherm from shelf depths deeper than 60 m to nearly 30 m (Figures 9 and 11). By approximately 19:00 on 15 October, the INL had spread approximately 2.7 km offshore (westward). The stretching and straining caused by the down-slope movement of warmer, nearshore waters in response to the wind reversal may have caused a flux convergence of SPM, causing the material to spread alongisopycnal, offshore from the shelf. This suggests that the unbalanced water column response to wind relaxations may drive compression and extension between isotherms that, in turn, can cause suspended material near the seabed to be "pinched off" into an INL that then dispersed laterally offshore. This would represent another possible transport mechanism for SPM on the shelf.

[45] **Acknowledgments.** This project was funded by the National Science Foundation (grant OCE0961810 to McPhee-Shaw, Bellingham, Shaw, and Stanton), and by the U.S. Geological Survey. Project Assistant C. Hunter (MLML) prepared and oversaw the deployment and recovery of the moored instrument platforms. B. Hobson oversaw deployment and operation of the LRAUV. D. Kolber (MBARI) helped prepare and post-process autonomous underwater vehicle data. We gratefully acknowledge M. McManus at the University of Hawaii at Manoa for loaning us the SeaHorse autonomous profiler and associated instrumentation. We thank K. Rosenberger for his contributions to and preliminary editing of this manuscript. J. Sevadjian and B. Raanan offered helpful suggestions for field work planning and data analyses. B. Edwards and J. Reid supplied the sediment grain size data shown in Figure 1, and N. Golden assisted with mapping this data. We thank the captain and crews of the RV *Pt Sur* and all the MLML students who assisted with field operations. The authors are very grateful to P. Puig and two anonymous reviewers, whose comments and suggestions greatly improved the manuscript.

References

Austin, J. A., and S. J. Lentz (2002), The inner shelf response to wind-driven upwelling and downwelling, *J. Phys. Oceanogr.*, *32*, 2171–2193.

Bogucki, D., T. Dickey, and L. G. Redekopp (1997), Sediment resuspension and mixing by resonantly generated internal solitary waves, *J. Phys. Oceanogr.*, *27*, 1181–1196.

Bourgault, D., M. Morsilli, C. Richards, U. Neumeier, and D. E. Kelley (2013), Sediment resuspension and nepheloid layers induced by long internal solitary waves shoaling orthogonally on uniform slopes, *Cont. Shelf Res.*, *72*, 21–33.

Breaker, L. C., and W. W. Broenkow (1994), The circulation of Monterey Bay and related processes, *Oceanogr. Mar. Biol.*, *32*, 1–64.

Bruland, K. W., E. L. Rue, and G. J. Smith (2001), Iron and macronutrients in California coastal upwelling regimes: Implications for diatom blooms, *Limnol. Oceanogr.*, *46*, 1661–1674.

Brun-Cottan, J. C., S. Guillou, and Z. H. Li (2000), Behavior of a puff of resuspended sediment: A conceptual model, *Mar. Geol.*, *167*, 355–373.

Cacchione, D. A., and D. E. Drake (1986), Nepheloid layers and internal waves over continental shelves and slopes, *Geo Mar. Lett.*, *6*, 147–152.

Cacchione, D. A., and J. B. Southard (1974), Incipient sediment movement by shoaling internal gravity waves, *J. Geophys. Res.*, *79*, 2237–2242.

Carter, G. S., M. C. Gregg, and R.-C. Lien (2005), Internal waves, solitary-like waves, and mixing on the Monterey Bay shelf, *Cont. Shelf Res.*, *25*, 1499–1520.

Cazenave, F., Y. Zhang, E. E. McPhee-Shaw, J. G. Bellingham, and T. P. Stanton (2011), High-resolution surveys of internal tidal waves in Monterey Bay, California, using an autonomous underwater vehicle, *Limnol. Oceanogr. Methods*, *9*, 571–581.

Chelton, D. B., R. A. deSzoeke, and M. G. Schlax (1998), Geographical variability of the first baroclinic Rossby radius of deformation, *J. Phys. Oceanogr.*, *28*, 433–460.

Cheng, R. T., C.-H. Ling, and J. W. Gartner (1999), Estimates of bottom roughness length and bottom shear stress in South San Francisco Bay, California, *J. Geophys. Res.*, *104*, 7715–7728.

Dickson, R. R., and I. N. McCave (1986), Nepheloid layers on the continental slope west of Porcupine Bank, *Deep Sea Res., Part A*, *33*, 791–818.

Donelan, M. A., J. Hamilton, and W. H. Hui (1985), Directional spectra for wind-generated waves, *Philos. Trans. R. Soc. London A*, *315L*, 509–562.

Dunbar, G. B., and P. J. Barrett (2005), Estimating palaeobathymetry of wave-graded continental shelves from sediment texture, *Sedimentology*, *52*(2), 253–269.

Durrieu de Madron, X. (1994), Hydrography and nepheloid structures in the Grande-Rhone canyon, *Cont. Shelf Res.*, *14*, 457–477.

Edwards, B. D. (2002), Variations in sediment texture on the northern Monterey Bay National Marine Sanctuary continental shelf, *Mar. Geol.*, *181*, 83–100.

Ferré, B., C. R. Sherwood, and P. L. Wiberg (2010), Sediment transport on the Palos Verdes shelf, California, *Cont. Shelf Res.*, *30*, 761–780.

Gardner, W. D. (1989), Periodic resuspension in the Baltimore canyon by focusing of internal waves, *J. Geophys. Res.*, *94*, 18,185–18,194.

George, D. A., and P. A. Hill (2008), Wave climate, sediment supply and the depth of the sand-mud transition: A global survey, *Mar. Geol.*, *254*, 121–128.

Holloway, P. E. (1987), Internal hydraulic jumps and solitons at a shelf break region on the Australian North West shelf, *J. Geophys. Res.*, *92*, 5405–5416.

Inall, M. (2009), Internal wave induced dispersion and mixing on a sloping boundary, *Geophys. Res. Lett.*, *36*, L05604, doi:10.1029/2008GL036849.

Inthorn, M., V. Mohrholz, and M. Zabel (2006), Nepheloid layer distribution in the Benguela upwelling area offshore Namibia, *Deep Sea Res., Part I*, *53*, 1423–1438.

Ivey, G. N., and R. I. Nokes (1989), Vertical mixing due to the breaking of critical internal waves on sloping boundaries, *J. Fluid Mech.*, *66*, 223–239.

Jachec, S. M., O. B. Fringer, M. G. Gerritzen, and R. L. Street (2006), Numerical simulation of internal tides and the resulting energetics within

Monterey Bay and the surrounding area, *Geophys. Res. Lett.*, *33*, L12605, doi:10.1029/2006GL026314.

Jachec, S. M. (2012), Power estimates associated with internal tides from the Monterey Bay area, *Oceanogr., 25*(2), 52–55.

Johnson, D. R., A. Weidemann, and W. S. Pegau (2001), Internal tidal bores and bottom nepheloid layers, *Cont. Shelf Res.*, *21*, 1473–1481.

Johnston, T. M. S., D. L. Rudnick, G. S. Carter, R. E. Todd, and S. T. Cole (2011), Internal tidal beams and mixing near Monterey Bay, *J. Geophys. Res.*, *116*, C03017, doi:10.1029/2010JC006592.

Key, S. A. (1999), Internal tidal bores in the Monterey canyon, MS thesis, Dep. of Oceanogr., Naval Postgrad. Sch., Monterey, Calif.

Klymak, J. M., and J. N. Moum (2003), Internal solitary waves of elevation advancing on a shoaling shelf, *Geophys. Res. Lett.*, *30*(20), 2045, doi:10.1029/2003GL017706.

Kunze E., L. K. Rosenfeld, G. S. Carter, and M. C. Gregg (2002), Internal waves in Monterey Submarine Canyon, *J. Phys. Oceanogr.*, *32*, 1890–1913.

Kunze, E., C. MacKay, E. E. McPhee-Shaw, P. Chua, E. Kingsley, M. Denny, R. Phillips, S. J. Bograd, L. D. Zeidberg, and W. F. Gilly (2012), On the efficiency of mixing in bottom boundary layers over sloping topography, *J. Phys. Oceanogr.*, *42*, 910–926.

Largier, J. L., B. A. Magnell, and C. D. Winant (1993), Subtidal circulation over the Northern California Shelf, *J. Geophys. Res.*, *98*, 18,147–18,179.

Lucas, A. J., P. J. S. Franks, and C. L. Dupont (2011), Horizontal internal-tide fluxes support elevated phytoplankton productivity over the inner continental shelf, *Limnol. Oceanogr. Methods*, *1*, 56–74.

Lynch, J. F., J. D. Irish, C. R. Sherwood, Y. G. Agrawal (1994), Determining suspended sediment particle size information from acoustical and optical backscatter measurements, *Cont. Shelf Res.*, *14*, 1139–1165.

Madsen, O. S. (1994), Spectral wave-current bottom boundary layer flows, in *Proceedings of the 24th International Conference on Coastal Engineering*, vol. 1, pp. 384–398, Am. Soc. of Civ. Eng., Kobe, Japan.

McCave, I. N., I. R. Hall, A. N. Antia, L. Chou, F. Dehairs, R. S. Lampitt, L. Thomsen, T. C. E. van Weering, and R. Wollast (2001), Distribution, composition and flux of particulate material over the European margin at 47°–50°N, *Deep Sea Res., Part II*, *48*, 3107–3139.

McPhee-Shaw, E. E. (2006), Boundary-interior exchange: Reviewing the idea that internal-wave mixing enhances lateral dispersal near continental margins, *Deep Sea Res., Part II*, *53*, 42–59.

McPhee-Shaw, E. E., and E. Kunze (2002), Boundary layer intrusions from a sloping bottom: A mechanism for generating intermediate nepheloid layers, *J. Geophys. Res.*, *107*(C6), 3050, doi:10.1029/2001JC000801.

McPhee-Shaw, E. E., R. W. Sternberg, B. Mullenbach, and A. S. Ogston (2004), Observations of intermediate nepheloid layers on the northern California continental margin, *Cont. Shelf Res.*, *24*, 693–720.

Morrice, K. J. (2011), Dynamics of bottom boundary layer thickness in Monterey Bay canyon, MS thesis, Moss Landing Mar. Labs, Moss Landing, Calif.

Moum, J. N., J. M. Klymak, J. D. Nash, A. Perlin, and W. D. Smyth (2007), Energy transport by nonlinear internal waves, *J. Phys. Oceanogr.*, *37*, 1968–1988.

Nam, S., and U. Send (2011), Direct evidence of deep water intrusions onto the continental shelf via surging internal tides, *J. Geophys. Res.*, *116*, C05004, doi:10.1029/2010JC006692.

Nash, J. D., E. L. Shroyer, S. M. Kelly, M. E. Inall, T. F. Duda, M. D. Levine, N. L. Jones, R. C. Musgrave (2012), Are any coastal internal tides predictable? *Oceanogr.*, *25*(2), 80–95.

Nédélec, F., P. J. Statham, and M. Mowlem (2007), Processes influencing dissolved iron distributions below the surface at the Atlantic Ocean-Celtic Sea shelf edge, *Mar. Chem.*, *106*, 365–379.

Noble, M., and J. P. Xu (2003), Observations of large-amplitude cross-shore internal bores near the shelf break, Santa Monica Bay, CA, *Mar. Environ. Res.*, *56*, 127–149.

Oliver, J., K. Hammerstrom, E. McPhee-Shaw, P. Slattery, J. Oakden, S. Kim, and S. I. Hartwell (2011), High species density patterns in macrofaunal invertebrate communities in the marine benthos, *Mar. Ecol.*, *32*, 278–288.

Pak, H., and J. R. V. Zaneveld (1977), Bottom nepheloid layers and bottom mixed layers observed on the continental shelf off Oregon, *J. Geophys. Res.*, *82*, 3921–3931.

Pak, H., R. V. Zaneveld, and J. Kitchen (1980), Intermediate nepheloid layers observed off Oregon and Washington, *J. Geophys. Res.*, *85*, 6697–6708.

Palanques, A., and P. E. Biscaye (1992), Patterns and controls of the suspended matter distribution over the shelf and upper slope south of New England, *Cont. Shelf Res.*, *12*, 557–600.

Pennington, J. T., and F. P. Chavez (2000), Seasonal fluctuations of temperature, salinity, nitrate, chlorophyll and primary production at station H3/M1 over 1989–1996 in Monterey Bay, California, *Deep Sea Res., Part II*, *47*, 947–973.

Petruncio, E. T. (1993), Characterization of tidal currents in Monterey Bay from remote and in-situ measurements, MS thesis, Dep. of Oceanogr., Naval Postgrad. Sch., Monterey, Calif.

Petruncio, E. T., L. K. Rosenfeld, and J. D. Paduan (1998), Observations of the internal tide in Monterey canyon, *J. Phys. Oceanogr.*, *28*, 1873–1903.

Puig, P., J. B. Company, F. Sarda, and A. Palanques (2001), Responses of deep-water shrimp populations to intermediate nepheloid layer detachments on the Northwestern Mediterranean continental margin, *Deep Sea Res., Part I*, *48*, 2195–2207.

Puig, P., A. Palanques, J. Guillen, and M. El Khatab (2004), Role of internal waves in the generation of nepheloid layers on the northwestern Alboran slope: Implications for continental margin shaping, *J. Geophys. Res.*, *109*, C09011, doi:10.1029/2004JC002394.

Ribo, M., P. Puig, J. Salat, and A. Palanques (2013), Nepheloid layer distribution in the Gulf of Valencia, northwestern Mediterranean, *J. Mar. Syst.*, 111–112, 130–138.

Rosenfeld, L. K., F. B. Schwing, N. Garfield, and D. E. Tracy (1994), Bifurcated flow from an upwelling center: A cold water source for Monterey Bay, *Cont. Shelf Res.*, *14*(9), 931–964.

Rosenfeld, L.K., J. D. Paduan, E. T. Petruncio, J. E. Goncalves (1999), Numerical simulations and observations of the internal tide in a submarine canyon, *Proceedings of the 11th 'Aha Huliko'a Hawaiian Winter Workshop*, Dynamics of Internal Gravity Waves II, Honolulu, Hawaii, pp. 63–71.

Rosenfeld, L. K., I. Shulman, M. Cook, J. Paduan, and L. Shulman (2009), Methodology for a regional tidal model evaluation, with application to central California, *Deep Sea Res., Part II*, *56*(3), 199–218.

Rouse, H. (1937), Modern conceptions of the mechanics of fluid turbulence, *Trans. Am. Soc. Civ. Eng.*, *102*, 463–543.

Ryan, J. P., S. B. Johnson, A. Sherman, K. Rajan, F. Py, H. Thomas, J. B. L. Harvey, L. Bird, J. D. Paudan, and R. C. Vrijenhoek (2010), Mobile autonomous process sampling within coastal ocean observing systems, *Limnol. Oceanogr. Methods*, *8*, 394–402.

Sherwood, C. R., and L. F. Hibler (1994), Appendix D: Palos Verdes shelf wave modeling, in *Predictive Modeling of the Natural Recovery of the Contaminated, Effluent-Affected Sediment, Palo Verdes Margin, Southern California*, edited by D. E. Drake et al., pp. 42 + appendices, Battelle Mar. Sci. Lab., Sequim, Wash.

Skogsberg, T. (1936), Hydrography of Monterey Bay, California, thermal conditions, 1929–1933, *Trans. Am. Philos. Soc.*, *29*(1), 1–152.

Soulsby, R.L. (1997), *Dynamics of Marine Sands*. Thomas Telford, London.

Stanton, T. P., and L. Ostrovsky (1998), Observations of highly nonlinear, tidally forced solitons over the continental shelf, *Geophys. Res. Lett.*, *25*, 2695–2698.

Sternberg, R. W. S., and L. H. Larsen (1975), Frequency of sediment movement on the Washington continental shelf: A note, *Mar. Geol.*, *21*, M37–M47.

Sternberg, R. W. S., I. Berhane, and A. S. Ogston (1999), Measurement of size and settling velocity of suspended aggregates on the northern California continental shelf, *Mar. Geol.*, *154*, 43–53.

Storlazzi, C. D., and J. A. Reid (2010), The influence of El Nino-Southern Oscillation (ENSO) cycles on wave-driven sea-floor sediment mobility along the central California continental margin, *Cont. Shelf Res.*, *30*, 1582–1599.

Storlazzi, C. D., M. A. McManus, and J. D. Figurski (2003), Long-term, high-frequency current and temperature measurements along central California: Insights into upwelling/relaxation and internal waves on the inner shelf, *Cont. Shelf Res.*, *23*, 901–918.

Storlazzi, C. D., J. A. Reid, and N. E. Golden (2007), Wave-driven spatial and temporal variability in the sea-floor sediment mobility in the Monterey Bay, Cordell Bank, and Gulf of the Farallones National Marine Sanctuaries, *Sci. Invest. Rep. 2007–5233*, U.S. Geol. Surv., Santa Cruz, Calif.

Taylor, J. R. (1993), Turbulence and mixing in the boundary layer generated by shoaling internal waves, *Dyn. Atmos. Oceans*, *19*, 233–258.

Torrence, C., and G. P. Compo (1998), A practical guide to wavelet analysis, *Bull. Am. Meteorol. Soc.*, *79*, 61–78.

Trowbridge J. H., A. R. M. Nowell (1994), An introduction to the Sediment Transport Events on Shelves and Slopes (STRESS) Program, *Cont. Shelf Res.*, *14*, 1057–1061.

Walsh, J. P., and C. A. Nittrouer (1999), Observations of sediment flux to the Eel continental slope, northern California, *Mar. Geol., 154*(1–4), 55–68.

Walter, R. K., C. B. Woodson, R. S. Arthur, O. B. Fringer, and S. G. Monismith (2012), Nearshore internal bores and turbulent mixing in southern Monterey Bay, *J. Geophys. Res.*, *117*, C07017, doi:10.1029/2012JC008115.

Wang, X., Y. Chao, C. Dong, J. Farrara, Z. Li, J. C. McWilliams, J. D. Paduan, and L. K. Rosenfeld (2009), Modeling tides in Monterey Bay, California, *Deep Sea Res., Part II*, *56*, 219–231.

Watson, F., M. Angelo, T. Anderson, J. Casagrande, D. Kozlowski, W. Newman, J. Hager, D. Smith, and B. Curry (2003), Salinas valley sediment sources, *Cent. Coast Watershed Stud. Rep. WI-2003-06*, Watershed Inst., Seaside, Calif.

Wiberg, P. L., and C. R. Sherwood (2008), Calculating wave-generated bottom orbital velocities from surface-wave parameters, *Comput. Geosci.*, *34*, 1243–1262.

Woodson, C. B., et al. (2011), Observations of internal wave packets propagating along-shelf in northern Monterey Bay, *Geophys. Res. Lett.*, *38*, L01605, doi:10.1029/2010GL045453.

van Leussen, W. (1999), The variability of settling velocities of suspended fine-grained sediment in the Ems estuary, *J. Sea Res.*, *41*, 109–118.

van Weering, T. C. E., et al. (2001), Benthic dynamics and carbon fluxes on the NW European continental margin, *Deep Sea Res., Part II*, *48*, 3191–3221.

Xu, J., J. Xie, and S. Cai (2011), Variation of Froude number versus depth during the passage of internal solitary waves form the in-situ observation and a numerical model, *Cont. Shelf Res.*, *31*, 1318–1323.

Xu, J. P., M. Noble, S. L. Eittreim, L. K. Rosenfeld, F. B. Schwing, and C. H. Pilskaln (2002), Distribution and transport of suspended particulate matter in Monterey Canyon, California, *Mar. Geol.*, *181*, 215–234.